

Chapter 17

Very High-Cycle Fatigue Resistance of Shot Peened High-Strength Aluminium Alloys: Role of Surface Morphology

M. Benedetti, V. Fontanari, and M. Bandini

Abstract The present paper is aimed at investigating the effect of shot peening on the very-high cycle fatigue resistance of the Al-7075-T651 alloy. Pulsating bending fatigue tests ($R = 0.05$) were carried out on smooth samples exploring fatigue lives comprised between 10^5 and 10^8 cycles. Three peening treatments with different intensity were considered to explore different initial residual stress profiles and surface microstructural conditions. An extensive analysis of the residual stress field was carried out by measuring with the X-ray diffraction (XRD) technique the residual stress profile before and at the end of the fatigue tests, so as to investigate the onset of a stabilized residual stress field. Fatigue crack initiation sites have been investigated through scanning electron microscopy (SEM) fractography. The surface morphology modifications induced by shot peening were evaluated using an optical profilometer. The influence of surface finishing on the fatigue resistance was quantified by eliminating the surface roughness in some peened specimens through a tribofinishing treatment.

Keywords Shot peening • Very high-cycle fatigue • Al-7075-T651 • Residual stresses • Tribofinishing

17.1 Introduction

Aluminium alloys are an attractive class of materials for aircraft and automotive industry because of their high specific static strength. In aerospace, aluminium alloys face ever stiffer competition from composites. In the automotive context, more and more engine parts are being made from them. Usually, high static mechanical properties are induced in aluminium alloys by dispersion hardening through solution and ageing heat treatments. However, aluminium alloys exhibit poor plain fatigue resistance and high notch fatigue sensitivity. Accordingly, stress raisers, like holes, fillets and grooves, always present in machine parts, are particularly detrimental to the fatigue response of these alloys, thus limiting their use in highly stressed mechanical components characterized by complex shapes. For this reason, aluminium alloys are frequently subjected to shot peening, particularly effective in incrementing the plain and notch fatigue strength of steels and light alloys. The shot peening mainly results in three fatigue related modifications of the surface layers: roughness, residual stresses and work hardening. Clearly, the surface roughening after shot peening is detrimental to the fatigue resistance due to the stress concentration exerted by the surface dimples. In the literature, it is commonly accepted that the improvement of fatigue strength is mainly induced by the introduction of compressive residual stresses in the surface region, responsible for both retarded fatigue crack initiation and lower small crack growth rates [1, 2]. The role of work hardening on the fatigue response is essentially indirect, since it strongly affects the stability of residual stresses by preventing them from relaxing due to accumulation of plastic deformation [3].

The authors recently studied the effect of three types of shot peening treatments on the plain and notch high-cycle fatigue response of the Al-7075-T651 alloy ($R = -1$) [4–8]. In particular, it was shown that (i) residual stress relaxation occurs when the superposition between the compressive residual stress and the compressive peak stress produced by reverse bending

M. Benedetti (✉) • V. Fontanari
Department of Industrial Engineering, University of Trento, via Mesiano 77, Trento 38100, Italy
e-mail: matteo.benedetti@ing.unitn.it

M. Bandini
Peen Service s.r.l., via Pollastri 7, Bologna 40138, Italy
e-mail: m.bandini@peenservice.it

exceeds the material's cyclic yield stress; (ii) the plain fatigue response is directly correlated with the surface residual stress as successfully predicted using a multiaxial fatigue criterion incorporating the stabilized residual stress field as mean stresses; (iii) gentle peening treatments conducted using small ceramic beads are more effective than more intense treatments employing larger peening media (iv) shot peening reduces the fatigue notch sensitivity; (v) the notch fatigue resistance can be satisfactorily predicted by the a multiaxial fatigue criterion incorporating stabilized residual stresses and combined with a line method based on the critical distance theory to account for the notch sensitivity. However, the current state-of-the-art-knowledge lacks for investigations proving whether the beneficial effect of shot peening is still present in the very-high cycle fatigue regime.

The present paper is aimed at investigating the effect of shot peening on the very-high cycle fatigue resistance of the Al-7075-T651 alloy. Pulsating bending fatigue tests ($R = 0.05$) were carried out on smooth samples exploring fatigue lives comprised between 10^5 and 10^8 cycles. Three peening treatments with different intensity were considered to explore different initial residual stress profiles and surface microstructural conditions. An extensive analysis of the residual stress field was carried out by measuring with the X-Ray Diffraction (XRD) technique the residual stress profile before and at the end of the fatigue tests, so as to investigate the onset of a stabilized residual stress field. Fatigue crack initiation sites have been investigated through Scanning Electron Microscopy (SEM) fractography. The surface morphology modifications induced by shot peening were evaluated using an optical profilometer. The influence of surface roughness on the fatigue resistance was quantified by eliminating the surface roughness in some peened specimens through a tribofinishing process.

17.2 Materials and Experimental Procedures

The experimentation was performed on the aluminium alloy Al-7075-T651, widely used for aeronautical applications, supplied in the form of 4 mm thick rolled plate. The bulk material properties were determined on five standard monotonic tensile tests (initial strain rate of $1 \times 10^{-3} \text{ s}^{-1}$) performed in the longitudinal orientation. The results, summarized in Table 17.1, show a yield strength higher than 500 MPa, combined with a good ductility (total elongation of 16 %).

The fatigue characterisation was carried out on hourglass specimens whose geometry, according to the standard ISO 3928, is illustrated in Fig. 17.1. The microstructure has been tested with the stress axis parallel to the L-direction. The samples present a fillet radius large enough to make any notch fatigue effects negligible.

Part of the specimens was subjected to controlled shot peening: the parameters of the three peening treatments considered are summarized in Table 17.2. Each treatment was performed using non-metallic beads, which lend light alloys higher fatigue performance as compared with steel shots without introducing undesired galvanic effects [6]. The basic idea was (i) to apply a widely used commercial peening treatment, termed Z425, employing beads of medium-small size (diameter $150 \mu\text{m}$), which introduces some surface roughness and a deep cold worked layer (depth $100 \mu\text{m}$), (ii) to explore an innovative peening treatment, called B120, with small ceramic beads leading to a gentle and superficial effect, (iii) and finally to investigate a fine particle shot peening treatment, termed V40, with very fine glass beads, which is known to greatly enhance the fatigue resistance of aluminium alloys [9].

In order to investigate the effect of the surface roughness induced by shot peening on the fatigue strength, three specimens previously subjected to the treatment B120 and V40 were then subjected to tribofinishing using a controlled vibrating tank with an aqueous medium containing high quality granulates and additives (mainly surfactants). During the process, the

Table 17.1 Monotonic tensile properties of the Al-7075-T651 alloy

E (GPa)	$\sigma_{Y0.2}$ (MPa)	UTS (MPa)	σ_F (MPa)	T.E. (%)	R.A. (%)
73 (± 1)	510 (± 5)	580 (± 5)	780 (± 10)	16 (± 2)	22 (± 2)

E elastic modulus, $\sigma_{Y0.2}$ 0.2 % yield stress, *UTS* ultimate tensile strength, σ_F true fracture stress, *T.E.* total elongation, *R.A.* reduction in area

Fig. 17.1 Geometry of the smooth hourglass specimen used in this study for bending fatigue tests. All dimensions are given in mm

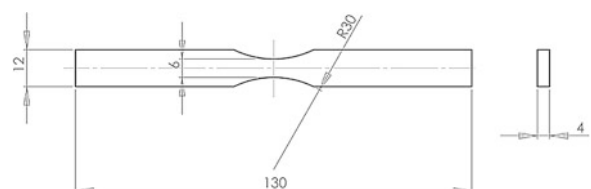
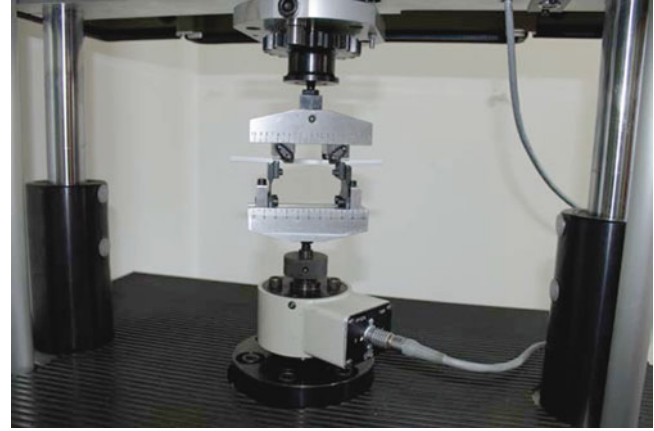


Table 17.2 Shot peening parameters

Treatment	Material	Bead size [μm]	Bead hardness [HV_1]	Bead composition	Almen intensity	Angle of impingement	Coverage [%]
Z150	Ceramic	150 \div 210	700	ZrO ₂ 67 %	12 N	90°	100
B120	Ceramic	63 \div 125		SiO ₂ 31 %	4.5 N		
V40	Glass	40 \div 70	550	SiO ₂ 31 % Na ₂ O 14 %	4.2 N		

Fig. 17.2 4-point bending fatigue test apparatus used in the present study

specimen surface was periodically observed with an optical microscope to make sure that polishing is stopped just after removing all the dimples created by the shot peening treatments. A material surface layer of approximately 5 \div 10 μm thickness was removed in this way.

Pulsating ($R = 0.05$) load-controlled 4-point bending fatigue tests were carried out in air, at room temperature, and at a nominal frequency of 110 Hz using a resonant testing machine Rumul Mikrottron 20 kN equipped with a 1 kN load cell (Fig. 17.2). Different stress levels corresponding to fatigue lives in the range between nearly 10^5 and 10^8 cycles were considered. Tests were terminated at 10^8 cycles when no fracture occurred. The fatigue curves corresponding to 50 % of failure probability, represented by the S-N curve:

$$\sigma_{P50} = \sigma_{0P50} \times N_f^{-\frac{1}{k}} \quad (17.1)$$

were determined by fitting the $\log(N_f)$ vs. $\log(\sigma)$ results. The uncertainty range was assumed to be constant and approximated by its centroid value. As a representative value of the scatter, the following expression was used:

$$T\sigma = 1 : \sigma_{P90}/\sigma_{P10} \quad (17.2)$$

P_{90} , P_{10} denote the 90 % and 10 % levels of failure probability, respectively.

The modifications of the surface layers produced by the shot peening treatments were investigated through microhardness, surface roughness and residual stress profile measurements. To this regard, microhardness profiles were measured to characterize the material's work hardening. Cross-sections were prepared by low-speed cutting with a diamond saw. To preserve the material work-hardening state, samples were cold-mounted in epoxy resin and then mechanically polished. A diamond Vickers indenter was used applying a maximum force of 1 N. The load was applied gradually at a constant 0.1 N/s rate with a dwell time of 10 s. Five measurements were performed at each depth and averaged in order to account for material's heterogeneity and measurement errors.

A confocal optical profilometer WLI Sensofar Plu Neox (plane surface spatial resolution of 0.31 μm , z-axial measurement resolution of 0.02 μm), was used to observe the samples surface. Three dimensional surface topography and roughness were evaluated.

Residual stress analysis was performed by X-Ray Diffraction (XRD) technique using an AST X-Stress 3000 X-ray diffractometer. Measurements were made with Cr K α radiation in the longitudinal direction in the gage region. The analysis zone was limited by a collimator of 1 mm² in area. The classical $\sin^2\psi$ method was applied for stress evaluation with the use of nine diffraction angles (2θ) scanned between -45° and $+45^\circ$ for each stress value. The $\{311\}$ diffracting planes were chosen (i) in order to obtain high angle measurements (2θ angle 139.0°) with higher strain sensitivity, and (ii) because they

do not accumulate significant intergranular stresses and hence exhibit similar behavior as that of the bulk. Calibration of the system was checked by collecting a diffraction pattern from a standard polycrystalline Al powder prior to conducting the experiment. The in-depth measurements were conducted step-by-step using an electro-polishing device by removing a very thin layer of material in a region (2 mm × 2 mm) localized at the gauge section of the specimens.

Both initial and stabilized residual stress fields were measured. For this purpose, measurements were performed on tested smooth specimens after failure in a region far enough from the fracture surface (about 2 mm) so that the material rupture was supposed not to have altered the residual stress field [4]. Measurements were carried out on both specimen sides, subjected to tensile and compressive bending stresses, respectively.

17.3 Results and Discussion

17.3.1 Surface Characteristics

The effect on the surface roughness exerted by the shot peening treatments is quantified in Table 17.3, where the results of the optical profilometer measurements made on an assessment area $636 \times 477 \mu\text{m}^2$ are summarized. It can be noted that the shot peening treatments increase the surface roughness with the respect to the as-received condition and that the most intense treatment Z150 results in a larger roughness increment with respect to the gentler processes B120 and V40. The tribofinishing is able to reduce the surface roughness of the peened samples below that of the virgin material. The as-received and the peened variants have a skewness close to zero, index of a symmetric height distribution (i.e. with as many peaks as valleys), while the tribofinished conditions have a negative skewness due to the fact that the surface asperities were removed by the polishing process. The maximum peak to valley height (S_z) and the mean spacing between profile peaks (D_p) can be used to estimate the stress concentration effect exerted by the surface dimples caused by shot peening according to the following expression proposed by [10]:

$$K_t = 1 + 4 \left(\frac{S_z}{D_p} \right)^{1.3} \quad (17.3)$$

The surface morphology of the virgin, Z150, B120, tribofinished B120, V40 and tribofinished V40 conditions is depicted in Fig. 17.3, respectively. Notably, the surface morphology of the as-received condition is characterized by striations caused by the rolling process. The large beads used in the most intense peening treatment, i.e. Z150, created large and deep impact craters. Dimples of smaller size, typical of gentle superficial peening treatments, are visible on the surfaces of the B120 and V40 conditions. The superficial structure of impact craters is not visible on the tribofinished variants.

The surface morphology of the virgin, Z150, B120, tribofinished B120, V40 and tribofinished V40 conditions is depicted in Fig. 17.3, respectively. Notably, the surface morphology of the as-received condition is characterized by striations caused by the rolling process. The large beads used in the most intense peening treatment, i.e. Z150, created large and deep impact craters. Dimples of smaller size, typical of gentle superficial peening treatments, are visible on the surfaces of the B120 and V40 conditions. The superficial structure of impact craters is not visible on the tribofinished variants.

A comparison among the microhardness profiles measured for both the peening treatments and the as-received condition is illustrated in Fig. 17.4. Noticeable differences, which are directly correlated to the surface work hardening experienced by the material as well as to the depth of the surface layer interested by the plastic deformation, can be observed: B120 and V40

Table 17.3 3D surface roughness properties

Condition	S_a [μm]	S_q [μm]	S_z [μm]	S_{sk}	S_{ku}	S_{dr} [%]	S_{pk} [μm]	S_k [μm]	S_{vk} [μm]	D_p [μm]	K_t
As-received	0.29	0.38	1.44	0.19	5.98	1.10	0.59	0.81	0.41	–	–
Z150	3.79	4.83	21.29	0.29	8.60	40.61	8.09	11.56	3.56	200	1.22
B120	1.24	1.54	7.12	0.14	3.03	6.07	1.75	3.96	1.42	110	1.11
B120 trib.	0.19	0.26	0.99	–1.21	12.17	0.60	0.29	0.55	0.38	–	–
V40	1.33	1.66	7.66	–0.01	2.96	3.79	2.12	4.23	1.24	100	1.14
V40 trib.	0.17	0.23	0.87	–1.30	12.52	0.61	0.28	0.49	0.33	–	–

S_a average roughness, S_q root mean square roughness, S_z maximum peak to valley height, S_{sk} skewness, S_{ku} kurtosis, S_{dr} developed interfacial area ratio, S_{pk} reduced peak height, S_k core roughness depth, S_{vk} reduced valley depth, D_p mean spacing between profile peaks, K_t stress concentration factor due to surface roughness

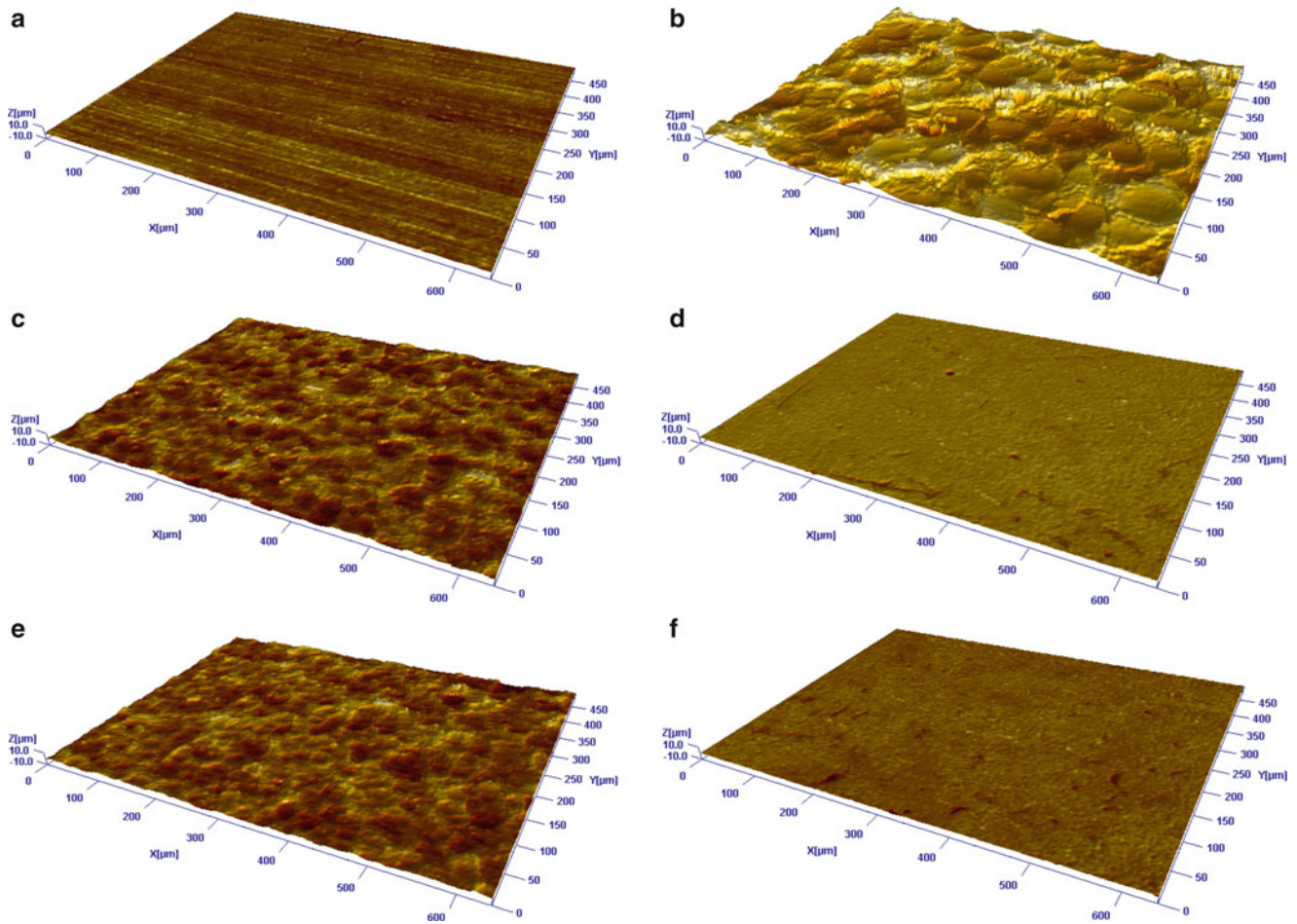
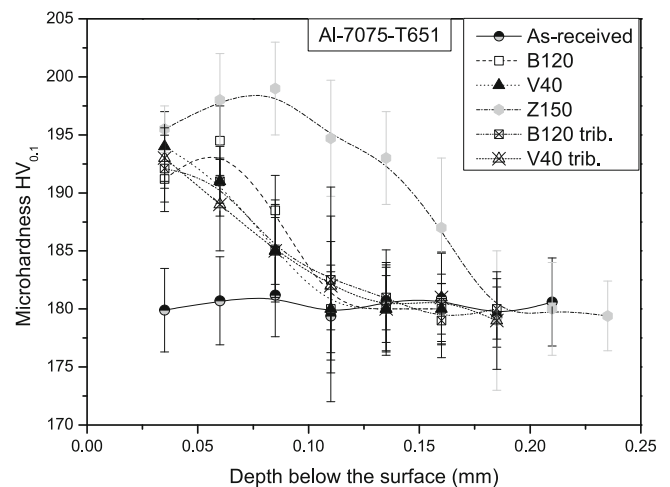


Fig. 17.3 Surface morphologies measured through optical profilometer. (a) As-received, (b) Z150 peened, (c) B120 peened, (d) B120 peened and tribofinished, (e) V40 peened, (f) V40 peened and tribofinished. The assessment area is $636 \times 477 \mu\text{m}^2$

Fig. 17.4 Microhardness profiles of the as-received and peened variants, obtained by averaging the results of five tests



peening treatments are very superficial, the maximum hardness is within $60 \mu\text{m}$ from the surface, the depth of the surface layer interested by the plastic deformation is about $100 \mu\text{m}$. The B120 treatment causes a more intense work hardening of the sub-superficial layers, and hence higher microhardness values, while the V40 treatment introduces higher microhardness values down to $40 \mu\text{m}$ below the surface. The Z150 treatment induces a sub-superficial microhardness peak, where the Hertzian pressure is nearly maximal; the effect of shot peening vanishes at approximately 0.17 mm below the surface. The tribofinishing treatment slightly modifies the microhardness profiles, mainly due to the removal of the outer material layer without significantly altering the work-hardening state.

Fig. 17.5 Initial residual stress profiles of the peened variants measured by XRD technique. Two measurements per peened variant were carried out in order to account for the variability in the residual stress field

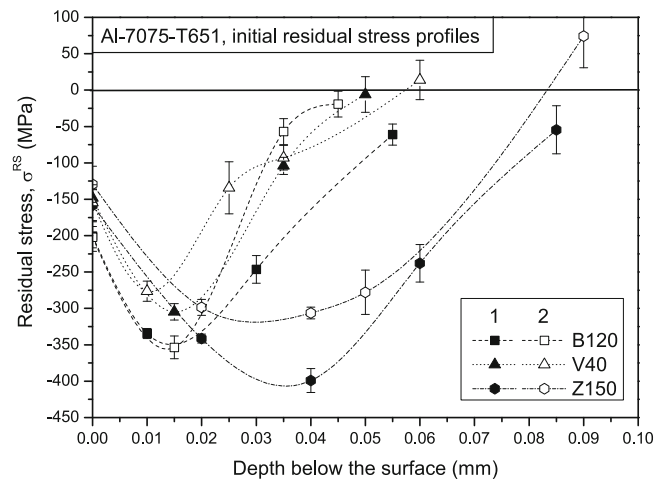
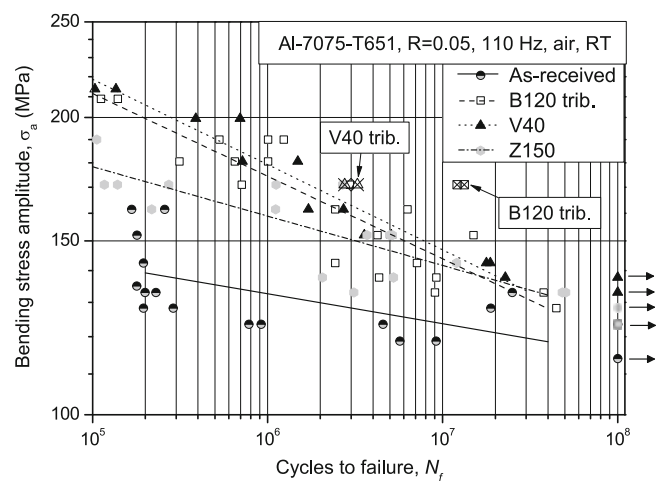


Fig. 17.6 Pulsating bending fatigue curves of the as-received and peened conditions. Run-out tests are marked by *arrows*



XRD measurements were carried out on the fatigue samples in order to characterize the residual stress field prior to fatigue testing. The obtained stress profiles are illustrated in Fig. 17.5. Two measurements per peening variant were performed in order to account for the variability in the residual stress field. The peening treatments B120 and V40 display a sub-superficial compressive residual stress peak located nearly $15 \mu\text{m}$ below the surface and a depth of the surface layer interested by compressive residual stresses equal to about $50 \mu\text{m}$. The B120 treatment induces higher residual stresses as compared with the V40 treatment. The most intense peening treatment Z150 is characterized by lower compressive surface residual stress, by higher sub-superficial compressive peak, and by deeper compressive residual stress profiles (about $90 \mu\text{m}$) with respect to the gentler treatments. The repeatability of the residual stress measurements is very good within a depth of about $20 \mu\text{m}$, where the fatigue response is mostly dictated [4], while it increases noticeably at higher depths, presumably due to the very elongated grain structure of the internal material layers that have not undergone recrystallization and hence grain refinement during shot peening.

17.3.2 Fatigue Curves

The results of the pulsating bending fatigue tests as well as the P50 fatigue lines are shown in Fig. 17.6 in the different material conditions considered and compared with those of the tests carried out on the two tribofinished variants. The parameters representing the fatigue curves corresponding to 50 % of failure probability, according to Eq. 17.1 and the results scatter, expressed by Eq. 17.2 are listed in Table 17.4.

All the peening treatments were effective in prolonging the fatigue life of the material as well as in reducing the large scatter in fatigue results displayed by the virgin material. This improvement depends on the applied load, being more remarkable for load levels corresponding to shorter fatigue lives, leading however to higher values of the slope in the P50

Table 17.4 Principal results of fatigue tests

Condition	k	σ_{0P50} [MPa]	$T\sigma$
As-received	33	200	1:1.22
Z150	20	315	1:1.17
B120	12	555	1:1.19
V40	12	590	1:1.10

k , σ_{0P50} slope and y-intercept of the Wöhler curve according to Eq. 17.1, $T\sigma$ results scatter according to Eq. 17.2

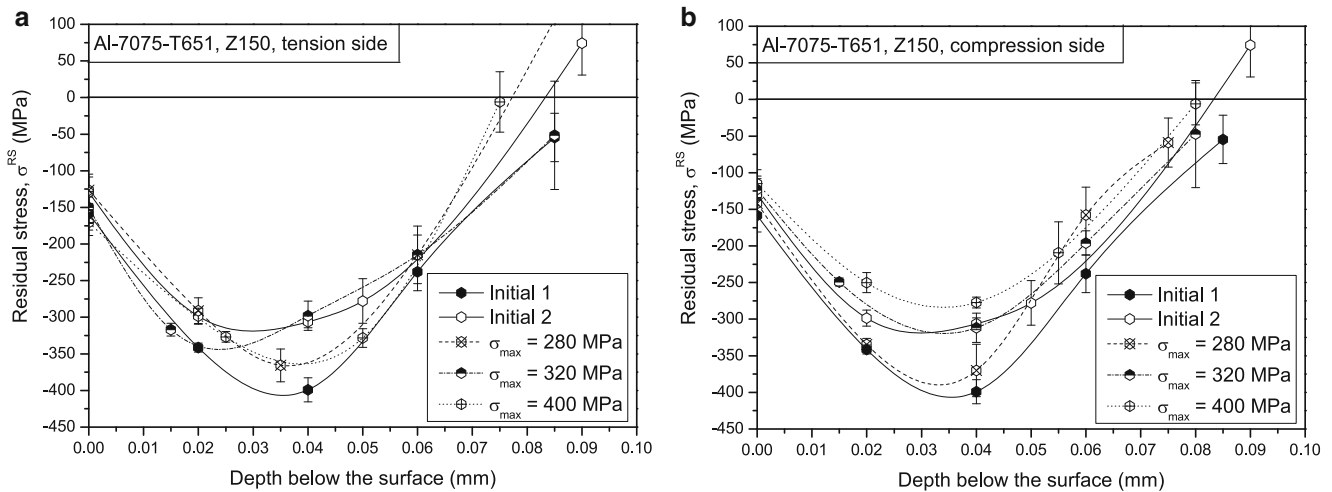


Fig. 17.7 Evolution of the residual stress profile during fatigue life in samples subjected to Z150 treatment. (a) Tensioned, (b) compressed side. Specimen tested at 280 (320, 400) maximum stress MPa failed after 50.6×10^6 (5.1×10^6 , 106,000) cycles

fatigue line. Therefore, the increment in fatigue resistance due to shot peening steadily declines during fatigue life. The lightest V40 peening treatment, despite lower surface residual stresses and slightly higher roughness, is more effective in improving the plain fatigue resistance with respect to the B120 treatment, which, in turn, performs better than the most intense treatment Z150. Finally, it can be noted that the tribofinished samples displayed a fatigue performance significantly higher with respect to the corresponding peened condition: the increment in fatigue strength due tribofinishing is about 5 % for the V40 and even 20 % for the B120 condition. The fact that the tribofinishing increments the fatigue performs of V40 in less extent than B120 condition suggests the hypothesis that the particular surface morphology of the V40 condition, characterized by lower values of developed interfacial area ratio and reduced valley depth, exerts a less detrimental effect on the fatigue response as compared with that exhibited by B120.

17.3.3 Residual Stress Evolution During Fatigue Life

Figures 17.7, 17.8 and 17.9 illustrate the evolution of the residual stress field at two loading levels for the Z150, B120 and V40 treatment, respectively. Figures 17.7 (17.8, 17.9) and 17.7 (17.8, 17.9) refer to the specimen surface subjected to compressive and tensile bending stresses, respectively. It can be noted that some relaxation of the residual stress field occurred on the outer layer of the specimen side subjected to compressive bending stresses, the more pronounced the higher the load levels, especially in the B120 and Z150 conditions. Conversely, significantly lower relaxation occurred on the specimen side subjected to tensile bending stresses. This confirm the observations made in [4, 5] that relaxation is more like a “quasi-static” effect, due to the achievement of the material’s plasticization when the compressive bending stresses are superimposed to the compressive surface residuals stress field. Cyclic relaxation seems to be negligible, since the application of tens of millions fatigue cycles do not significantly alter the surface residual stress field on the tensioned side of the samples.

Figure 17.10 illustrate the comparison between the initial (prior to tribofinishing) and the stabilized residual stress profiles for the tribofinished B120 and V40 variants, respectively. It can be noted that the material removal exposes on the surface the residual stress that was present at the corresponding depth prior to polishing. Moreover, tribofinishing caused some stress redistribution in the subsurface peak, while the depth of the surface layer interested by compressive residual

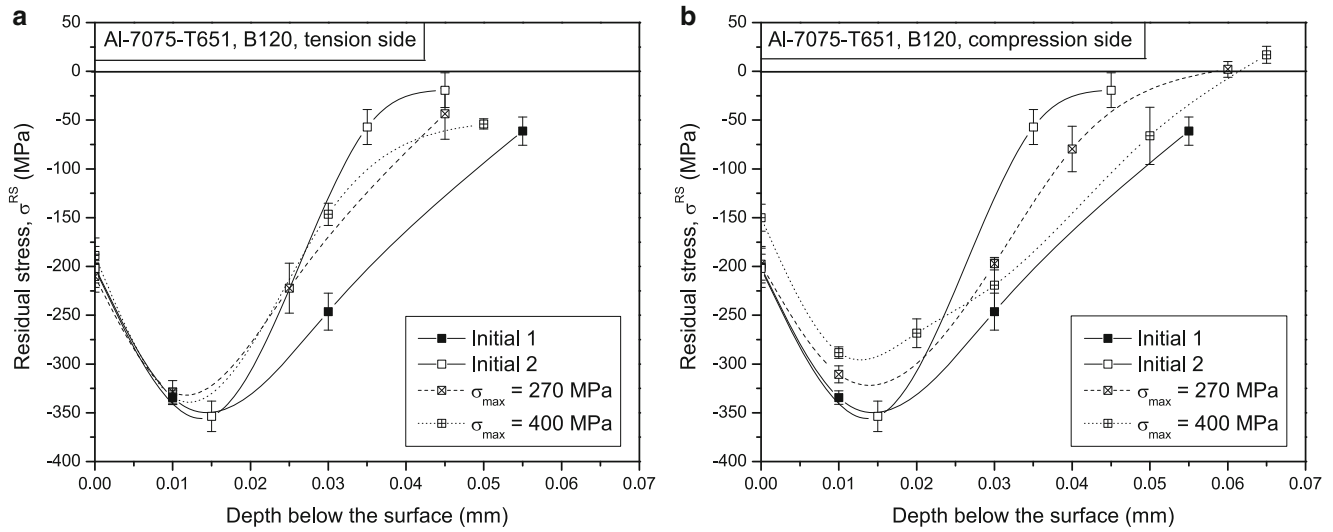


Fig. 17.8 Evolution of the residual stress profile during fatigue life in samples subjected to B120 treatment. (a) Tensioned, (b) compressed side. Specimen tested at 270 (400) maximum stress MPa failed after 44.6×10^6 (530,000) cycles

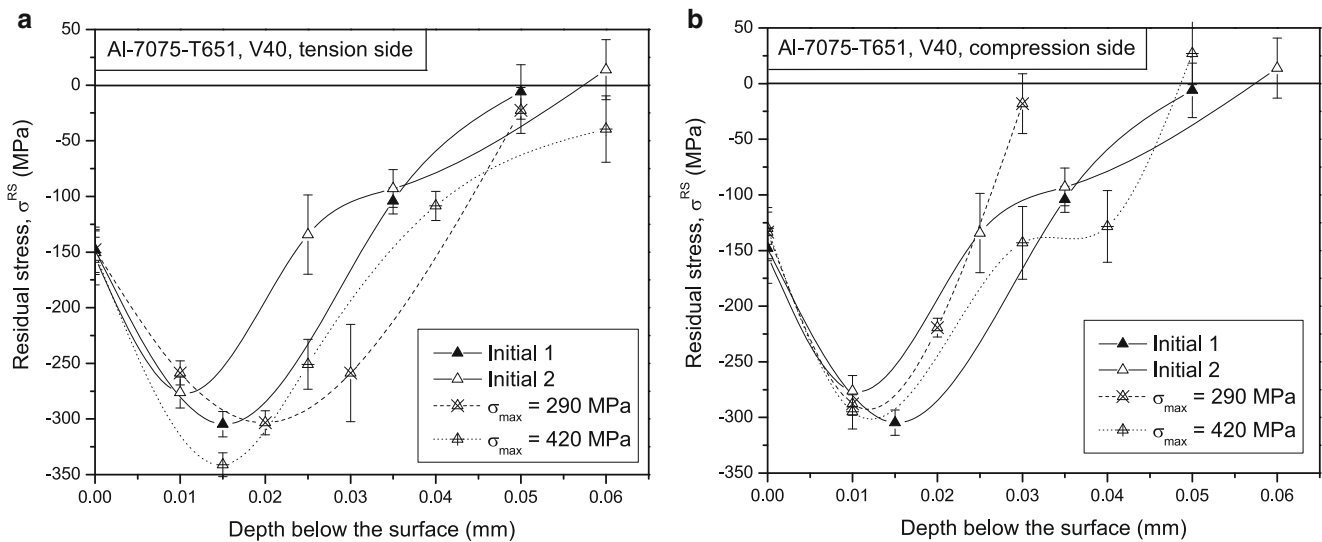


Fig. 17.9 Evolution of the residual stress profile during fatigue life in samples subjected to V40 treatment. (a) Tensioned, (b) compressed side. Specimen tested at 290 (420) MPa maximum stress failed after 22.8×10^6 (390,000) cycles

stresses remained nearly unaffected. Residual stress profiles are very similar on the tensioned and the compressed side of the specimen, thus suggesting that no residual relaxation occurred at the investigated stress level.

17.3.4 SEM Analysis of Fracture Surfaces

The fracture surfaces of all the fatigue samples were analyzed with the SEM. The analysis of the unpeened specimens revealed surface crack initiation throughout the entire fatigue life interval explored, even in the very high-cycle fatigue regime, as shown in Fig. 17.11. In the peened variants, surface crack initiation was found in the medium-cycle fatigue regime ($N_f < 1 \times 10^6$), as depicted in Fig. 17.11 for the B120 condition. At longer fatigue lives ($N_f > 2 \times 10^6$), almost all crack initiation sites were found below the surface. Moreover, the fracture surfaces near the crack initiation sites show several crystallographic planes. This is frequently observed in Al alloys when fatigue tests are conducted under vacuum and can be explained by the fact that the first propagation stages of sub-superficial cracks occur at very low partial pressures of

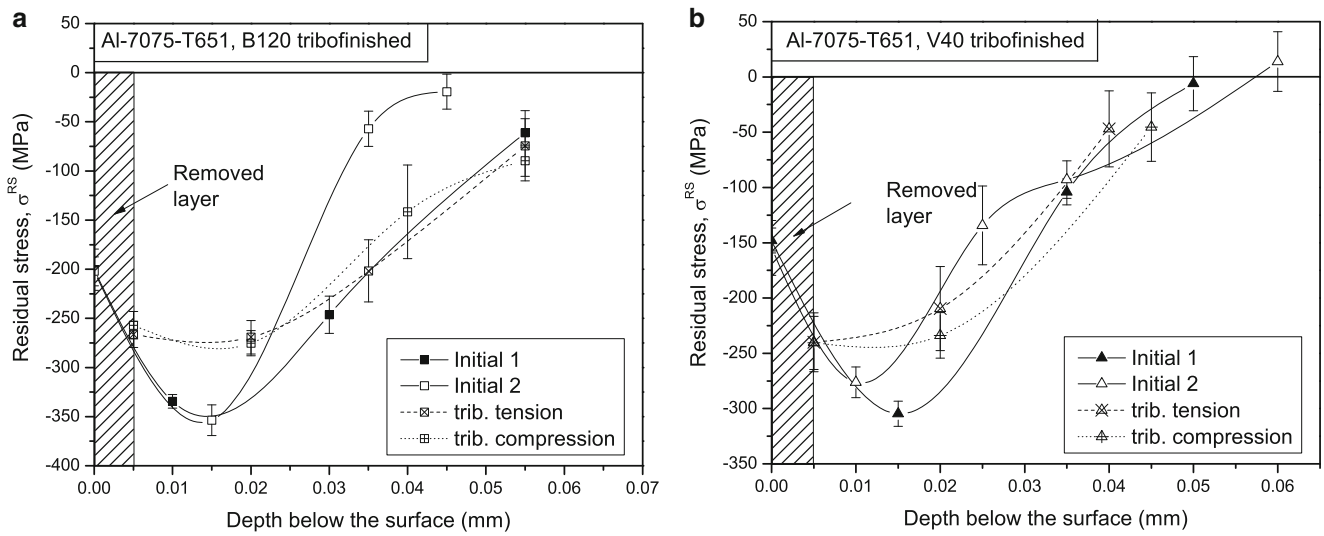


Fig. 17.10 Evolution of the residual stress profile during fatigue life in peened and tribofinished samples. (a) B120, (b) V40 peening. Specimens were tested at 360 MPa maximum stress and failed after (a) 13.3106 and (b) 3.3106 cycles

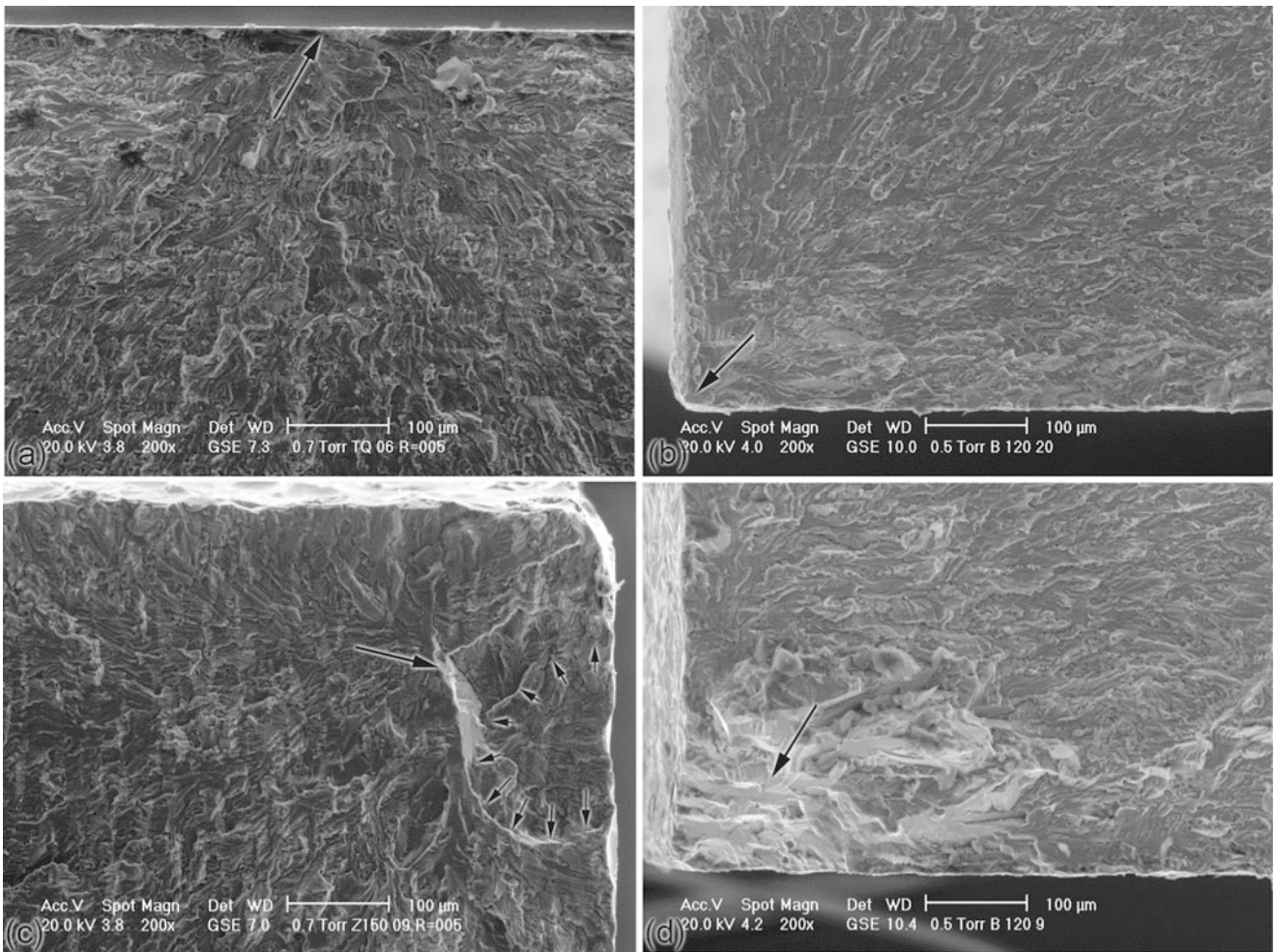


Fig. 17.11 SEM micrographs of the fracture surfaces around the fatigue crack initiation sites. (a) As-received ($\sigma_a = 133$ MPa, $N_f = 25.0 \times 10^6$), (b) B120 ($\sigma_a = 209$ MPa, $N_f = 139,000$), (c) Z150 ($\sigma_a = 133$ MPa, $N_f = 48.2 \times 10^6$), (d) B120 ($\sigma_a = 162$ MPa, $N_f = 6.3 \times 10^6$)

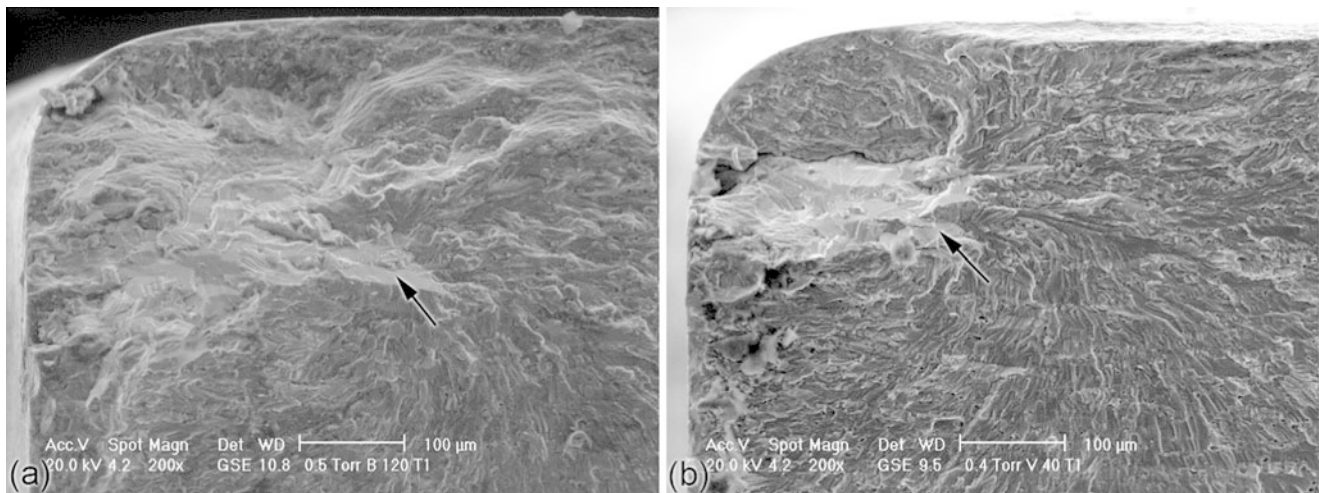


Fig. 17.12 SEM micrographs of the fracture surfaces around the fatigue crack initiation sites in the tribofinished specimens. Prior to tribofinishing the specimens were subjected (a) B120, (b) V40 peening treatment. Specimens were tested at $\sigma_a = 171$ MPa and failed after 13.3×10^6 and 3.3×10^6 cycles, respectively

oxygen. In general, specimens that failed at a number of cycles less than that corresponding to P50 probability show a non-propagating crack at the surface, near the subsuperficial initiation site of the main crack, as shown exemplarily in Fig. 17.11, while specimens that failed at a number of cycle significantly higher than that corresponding to P50 probability do not exhibit surface crack initiation, as depicted in Fig. 17.11. Apparently, non propagating cracks, initiated on the surface because of the stress concentration effect exerted by surface roughness, and arrested by the closing effect exerted by compressive residual stresses, promote crack initiation in the underlying layer, thus leading to a shorter fatigue life.

Figure 17.12 show the fracture surface of the tribonished B120 and V40 conditions, respectively. It can be noted that in both cases subsuperficial crack initiation occurred, but the extension of crystallographic crack growth is larger in the B120 than in the V40 condition. Apparently, the deeper compressive residual stress profile of the B120 condition was more effective in retarding crack propagation up to the surface than that of the V40 variant.

17.3.5 Simulation of the Fatigue Response

Recently, Benedetti et al. [8] conducted multiaxial fatigue tests on both unpeened and peened Al samples in order to identify the most suitable fatigue criterion. They found that the Crossland criterion was able to predict the fatigue strength with a relative error lower than 15 %, provided that the Stabilized Residual Stress (SRS) on the surface and the stress concentration factor due to surface roughness are considered. This approach clearly implies that the surface crack is the fatigue controlling parameter. In the present paper, the fatigue response of the peened samples has been predicted using the same material parameters of the Crossland fatigue criterion found in [8]. The SRS was assumed to depend on the applied external stress. For a given external stress level, the corresponding SRS was calculated by linearly interpolating the experimental values obtained at two stress levels on the tensioned side of the fatigue samples. Then, an iterative procedure was used to search for the SRS to be used in the fatigue criterion, in a similar way to that presented in [6, 7].

The comparison between the experimental data and the calculated mean fatigue curve is illustrated in Fig. 17.13 for the Z150, B120 and V40 conditions, respectively. The indication of the crack initiation site (superficial, subsuperficial or superficial assisted by a superficial non-propagating crack) of each fatigue tests is also provided. It can be noted that when the initiation of the dominant crack occurs on the surface, the agreement between experiments and predictions is very good, since the calculation model is based on the assumption of superficial crack initiation. On the contrary, if the shot peening treatment is able to suppress surface crack initiation and to push it beneath the layer affected by compressive residual stresses, as in the case of the tribofinished specimens and some specimens subjected to B120 and Z150 treatments, the predictions greatly underestimate the fatigue life. When the subsuperficial crack initiation is promoted by a non-propagating surface crack, the experiments are still in fairly good agreement with the prediction in the high-cycle fatigue regime ($N_f < 5 \times 10^6$), while the predictions underestimate the fatigue strength in the very high-cycle fatigue regime ($N_f > 10 \times 10^6$). Presumably,

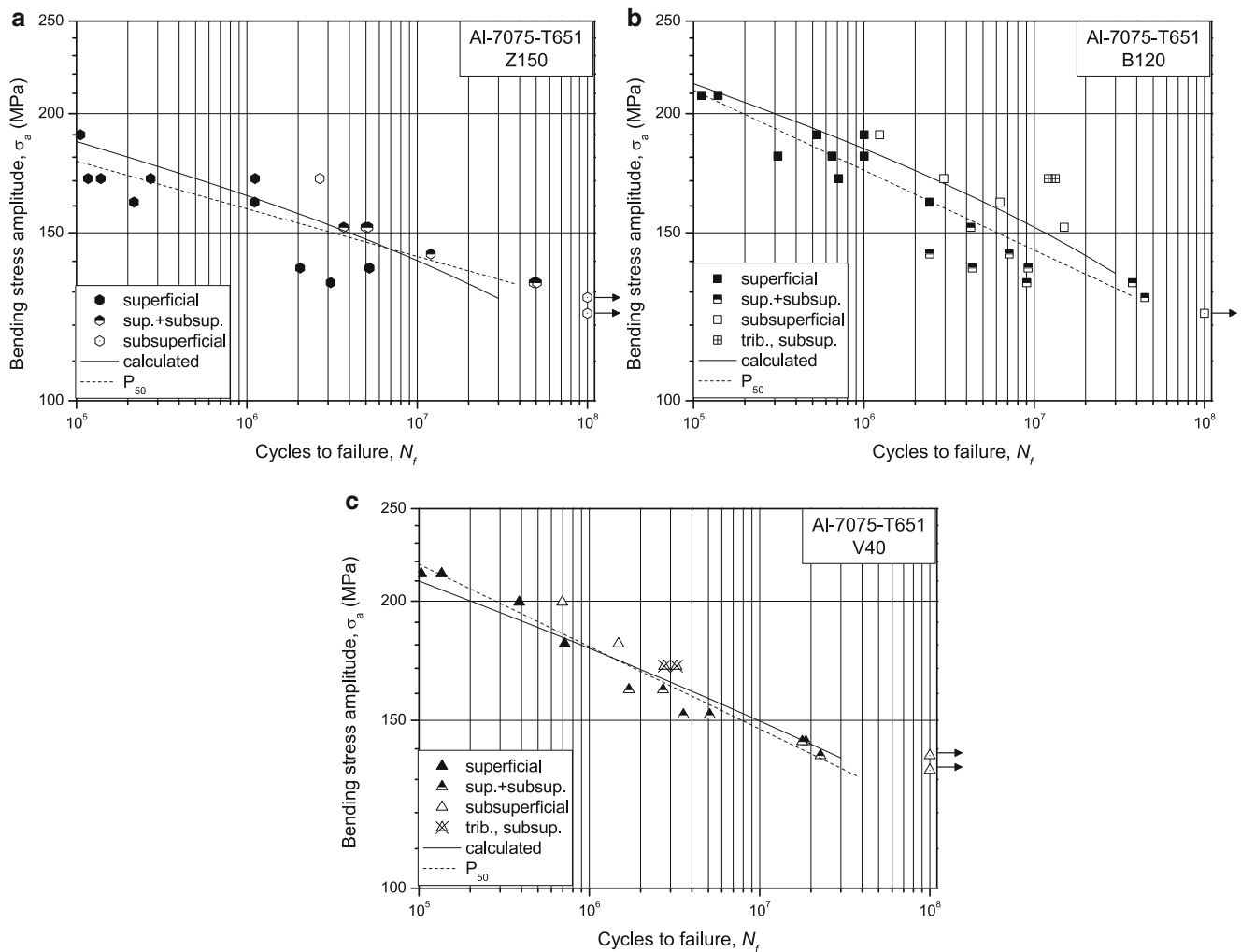


Fig. 17.13 Comparison between experimental and calculated P_{50} fatigue curves of the peened conditions. (a) Z150, (b) B120, and (c) V40 peening treatment. The experimental fatigue data are marked according to the crack initiation mechanism: (a) superficial crack initiation (*closed symbols*), (b) subsuperficial crack initiation (*open symbols*), (c) subsuperficial crack initiation promoted by a non-propagating surface crack (*half-closed symbols*)

in the former case, as soon as a crack initiates on the surface and is arrested, a crack quickly initiates below the surface leading to the sample fracture. In the latter case, a longer fatigue life is spent after surface crack arrest to initiate a superficial dominant crack.

17.4 Conclusions

The plain fatigue strength of shot peened aluminium alloy Al-7075-T651 was experimentally investigated exploring fatigue lives comprised between 10^5 and 10^8 cycles. Experiments were conducted on specimens subjected to three different shot peening treatments. The surface morphology was characterized using an optical profilometer. To quantify the influence of the change in surface morphology induced by shot peening upon the fatigue response, some peened samples were tribofinished with the aim of eliminating surface roughness and preserving the surface residual stress field. XRD measurements were carried out to determine the initial and the stabilized residual stress field. The following conclusions can be drawn:

1. Residual stress relaxation occurs mainly when compressive bending stresses are superimposed to the surface compressive residual stress field.

2. The effect exerted by shot peening is a complicated interaction between residual stresses and surface roughness, greatly impacting the mechanism of fatigue crack initiation and early propagation.
3. Shot peening conducted at low intensities with small beads is more effective in incrementing the fatigue resistance as compared to more intense treatments with larger shots, since it causes a lower roughening of the surface and induces the maximum compressive residual stress as close as possible to the surface where crack initiation is likely to occur.
4. In the very high cycle regime, the initiation of the crack leading to final failure occurs in the subsuperficial layers and may be promoted by the presence of non-propagating surface cracks. By eliminating surface roughness through a tribofinishing treatment, the occurrence of surface crack initiation is suppressed, thus further incrementing the beneficial effect of shot peening. The extent of this additional improvement depends on the type of shot peening treatment, being more significant if the layer interested by compressive residual stresses is deeper.

References

1. Guagliano M, Vergani L (2004) An approach for prediction of fatigue strength of shot peened components. *Eng Fract Mech* 71:501–512
2. Wagner L (1999) Mechanical surface treatments on titanium, aluminum and magnesium alloy. *Mater Sci Eng A* 263:210–216
3. McClung RC (2007) A literature survey on the stability and significance of residual stresses during fatigue. *Fatigue Fract Eng Mater Struct* 30:173–205
4. Benedetti M, Fontanari V, Scardi P, Ricardo CLA, Bandini M (2009) Reverse bending fatigue of shot peened 7075-T651 aluminium alloy: the role of residual stress relaxation. *Int J Fatigue* 31:1225–1236
5. Benedetti M, Fontanari V, Monelli BD (2010) Numerical simulation of residual stress relaxation in shot peened high-strength aluminium alloys under reverse bending fatigue. *ASME J Eng Mater Technol* 132:011012-1-9
6. Benedetti M, Fontanari V, Santus C, Bandini M (2010) Notch fatigue behaviour of shot peened high-strength aluminium alloys: experiments and predictions using a critical distance method. *Int J Fatigue* 32:1600–1611
7. Benedetti M, Fontanari V, Bandini M (2014) A simplified and fast method to predict plain and notch fatigue of shot peened high-strength aluminium alloys under reverse bending. *Surf Coat Technol* 243:2–9. doi:10.1016/j.surfcoat.2011.12.008
8. Benedetti M, Fontanari V, Bandini M, Taylor D (2014) Multiaxial fatigue resistance of shot peened high-strength aluminum alloys. *Int J Fatigue* 61:271–282
9. Oguri K (2011) Fatigue life enhancement of aluminum alloy for aircraft by Fine Particle Shot Peening (FPSP). *J Mater Proc Technol* 211:1395–1399
10. Li JK, Yao M, Wang D, Wang R (1992) An analysis of stress concentration caused by shot peening and its application in predicting fatigue strength. *Fatigue Fract Eng Mater Struct* 15(12):1271–1279